

# Redispersible Polymer Powders with High Bio-Based Content from Core–Shell Nanoparticles

Arianna Zanoni, Cora Casiraghi, Riccardo Po, Paolo Biagini, Mattia Sponchioni,\* and Davide Moscatelli

Redispersible polymer powders (RDPPs), i.e., additives obtained from core–shell nanoparticles and commercialized in the form of a dry powder, find intensive application in the concrete industry. However, they are mainly produced from fossil resources. Therefore, the development of bio-based RDPPs is important to reduce the carbon footprint of these additives. In this work, two types of core–shell nanoparticles with a high percentage of bio-based content are synthesized and show to be good candidates as RDPPs. In the first case, up to 75% of bio-based content is obtained by combining lauryl acrylate, derived from coconut and palm kernel oil, as main core material, with isobornyl methacrylate, coming from pine resin, exploited to create the outer harder shell. In the second case, a degradable macromonomer obtained by the ring opening polymerization of lactide using 2-hydroxyethyl methacrylate as initiator is used as the core-forming monomer to obtain degradable RDPPs. In both cases, the particles are synthesized with a two-step emulsion polymerization process conducted in one pot and then spray-dried to obtain the RDPPs of interest. The morphology and redispersibility of the powders are characterized. Finally, their use as concrete additives is preliminarily assessed by evaluating their effect on changes in the surface morphologies of concrete specimens.

## 1. Introduction

The invaluable properties of nanostructured polymer materials are known from decades. As a matter of fact, polymer latexes are nowadays applied in manifold everyday commodities, including paints and coatings,<sup>[1]</sup> adhesives,<sup>[2]</sup> and cosmetic and personal care products.<sup>[3,4]</sup>


However, a recurrent problem with these nanoparticles (NPs) is the modulation of their physicochemical properties to access complex behaviors and, in turn, to reach advanced applications. A potential solution is represented by core–shell NPs, which are gaining much interest due to their peculiar morphology, tunable properties by independently controlling the characteristics of the core and shell materials, and broad application range.<sup>[5]</sup> These core–shell NPs can comprise both organic and inorganic components, with the inorganic constituent usually made of titanium oxide, silica, or calcium carbonate that improve the mechanical strength, modulus, and thermal stability of the polymer used as organic component.<sup>[6–8]</sup>

When both the inner core and the outer shell are made of polymer materials, the core of the NPs is typically synthesized first, and the shell is grown on the core during a second polymerization stage. Most of the times, these nanostructured materials are obtained via free-radical emulsion polymerization, which is very advantageous in terms of high polymerization rate, narrow particle size distribution, and high molecular weight of the produced polymers. In this scenario, the shell is typically grown by exploiting the core as seed and paying particular attention to avoid re-nucleation, which would lead to an undesired mixture of colloids with their own peculiar properties.<sup>[9,10]</sup>

The synthesis of core–shell polymer NPs usually comes from the necessity of having different glass transition temperatures ( $T_g$ ) simultaneously in the same material:<sup>[11]</sup> depending on the applications, the core can be soft and the shell hard or vice versa.<sup>[9]</sup> This difference in the  $T_g$  can be advantageously exploited, for example, to produce the so-called redispersible polymer powders (RDPPs), hydrophobic polymer NPs sold in the form of a dry powder that can be easily resuspended in aqueous media to re-obtain the original properties.<sup>[12]</sup> The advantages of these powders are the easiness of transportation, that can be

A. Zanoni, C. Casiraghi, M. Sponchioni, D. Moscatelli  
 Department of Chemistry  
 Materials and Chemical Engineering “Giulio Natta”  
 Politecnico di Milano  
 via Mancinelli 7, Milano 20131, Italy  
 E-mail: mattia.sponchioni@polimi.it

R. Po, P. Biagini  
 Renewable, New Energy and Material Science Research Centre  
 Istituto Guido Donegani  
 Eni S.p.A.  
 via Fauser 4, Novara 28100, Italy

 The ORCID identification number(s) for the author(s) of this article can be found under <https://doi.org/10.1002/mame.202200443>

© 2022 The Authors. Macromolecular Materials and Engineering published by Wiley-VCH GmbH. This is an open access article under the terms of the Creative Commons Attribution License, which permits use, distribution and reproduction in any medium, provided the original work is properly cited.

DOI: 10.1002/mame.202200443

achieved at lower costs due to the compression of the volumes compared to the original latexes, and of mixing with other materials in addition to the possibility of resuspending the product at the required concentration. To obtain these RDPPs, a hard shell is required to avoid agglomeration and sticking during the drying process, typically occurring at high temperature. In fact, the low polymer chain mobility below their  $T_g$  limits the particle interpenetration and fusion, thus saving their identity. On the other hand, the inner core is typically a softer material, e.g., to improve the film forming ability.<sup>[13]</sup> After the water evaporation, the polymer film formation occurs enhancing properties like wear resistance, tensile and impact strength or water resistance. For these reasons, RDPPs are particularly appreciated in tile and construction adhesives, plasters, waterproofing, and crack isolation membranes and external wall putty.<sup>[14]</sup>

Even if polymer mixtures are added to concrete in a small percentage, usually ranging from 3% to 20%,<sup>[15]</sup> the concrete market is nowadays producing 4.1 billion metric tons worldwide,<sup>[16]</sup> leading to more than 120 million metric tons of additives, even considering to add the smallest amount possible. These additives are mostly produced from fossil resources, which has an impact on the carbon footprint of the concrete industry. The picture is then much worsened if energy considerations are introduced. Most of the RDPPs are produced by spray-drying, requiring an important amount of energy for water evaporation. Not to tell the extreme temperature conditions required in the clinker process. These combined aspects of high energy requirements and additives with fossil origin lead the concrete industry to be estimated as the responsible for the 8% of the global CO<sub>2</sub> emissions.<sup>[17]</sup>

Even if its impact could be limited, it has been already demonstrated that the use of bio-based additives can lower the concrete carbon footprint and environmental impact.<sup>[18]</sup> Nonetheless, this field is still poorly explored and, so far, the few available examples of bio-based materials comprise cellulose fibers added to improve the mechanical strength.<sup>[19]</sup> On the other hand, the market is still dominated by oil-based additives, mainly poly(vinyl acetate) (PVAc), alone<sup>[14]</sup> or copolymerized with ethylene,<sup>[15, 20]</sup> silanes,<sup>[21]</sup> styrene, and softer polymers like poly(2-ethylhexyl acrylate).<sup>[13]</sup> Therefore, the development of suitable bio-based materials as concrete additives, replacing those produced from fossil sources, is important to improve the environmental sustainability of the whole industrial sector at least from the material side.

In this work, we designed and investigated the use of core-shell polymer NPs with a high percentage of bio-based component as RDPPs to be exploited as concrete additives.

In a first formulation, we exploited lauryl acrylate (LA) to realize the soft core of the NPs. In fact, this is a bio-based monomer obtained by the esterification of acrylic acid and lauryl alcohol, that is the major component of coconut and palm kernel oil. Due to the low glass transition temperature of the corresponding polymer, it is already used to produce partially bio-based pressure sensitive adhesives.<sup>[22]</sup> On the other hand, isobornyl methacrylate (IBOMA), a monomer with 71% of its carbons coming from pine resin, was exploited to obtain the hard shell of the NPs. As a matter of fact, due to its high  $T_g$  of 125 °C, this monomer has been already investigated in the literature as potential substituent of methyl methacrylate.<sup>[22, 23]</sup>

As a further improvement to this formulation with >70% of components coming from natural sources, we investigated the

possibility of synthesizing bio-based and degradable core-shell NPs suitable for RDPPs. To access this characteristic, the particle core was synthesized from a lactic acid-based macromonomer produced via ring opening polymerization (ROP) of lactide initiated by 2-hydroxyethyl methacrylate (HEMA). The product is an oligoester, hereinafter HEMALA<sub>4</sub> (where 4 indicates the average number of lactoyl repeating units), that can undergo free-radical chemistry being at the same time composed by bio-renewable chemicals for the 67% of its carbons and degradable, as its ester bonds can be cleaved by hydrolysis. In particular, its degradation when formulated in polymer NPs has been previously studied by Yu et al.<sup>[24]</sup> Styrene instead was selected as the shell material, as particularly suitable for RDPP applications.<sup>[13]</sup>

In both cases, a one-pot free-radical emulsion polymerization in two steps was exploited to realize the core first, followed by the growth of the shell. Ammonium persulfate (APS) and sodium dodecyl sulfate (SDS) were used as initiator and ionic surfactant, respectively. Indeed, the use of a negatively charged stabilizer is proven to increase the interactions with the positively charged concrete and at the same time to favor the NP miscibility and make the additive work also as superplasticizers.<sup>[25]</sup>

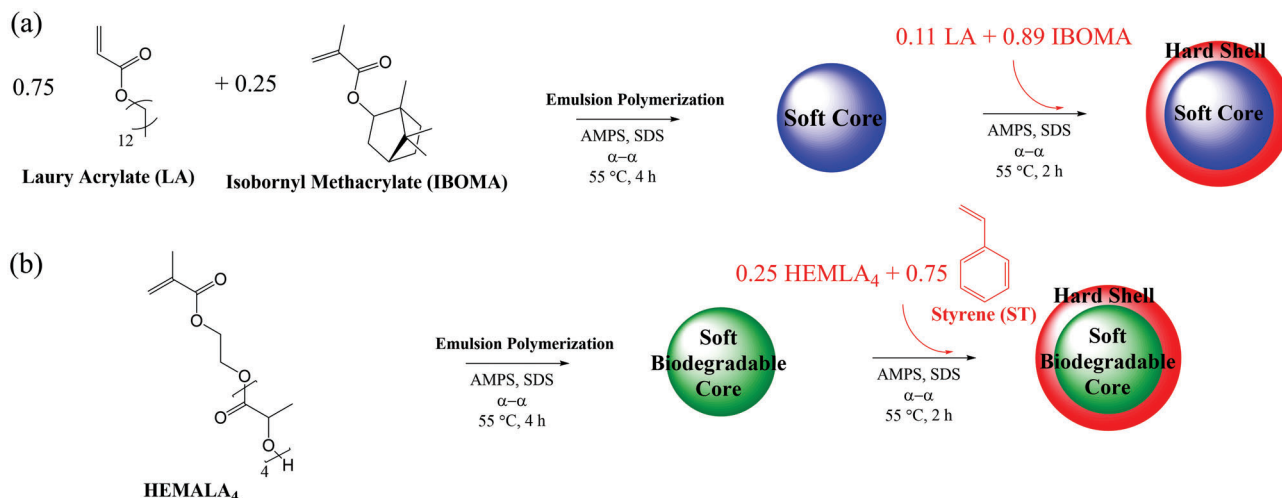
After the synthesis, the NPs were spray dried and the redispersibility in water, a key feature for RDPPs, was studied varying the shell thickness and the amount of protective agent. Finally, a preliminary test proved that the particles could create a homogenous dispersion in concrete. SEM and optical microscope images showed that in the case of the LA-IBOMA NPs a more compact waterproof surface was obtained. Instead, HEMALA<sub>4</sub>-styrene NPs increased the number of voids in the concrete, bringing about the possibility of being further studied as air-entrainment additives.

## 2. Experimental Section

### 2.1. Materials

Tin(II) 2-ethylhexanoate (stannous octoate, Sn(Oct)<sub>2</sub>, MW = 405.12 g mol<sup>-1</sup>), 3,6-dimethyl-1,4-dioxane-2,5-dione (lactide, Lac, 99%, MW = 144.13 g mol<sup>-1</sup>), 2,2-azobis(2-methylpropionamide) dihydrochloride ( $\alpha$ - $\alpha$ , 97%, MW = 271.19 g mol<sup>-1</sup>), ethanol (EtOH, 99.8%, MW = 46.07 g mol<sup>-1</sup>), styrene (ST, 99.5% stab. with 10–15 ppm 4-t-butylcatechol), 1,2-ethanediol mono(2-methylpropenoate) (HEMA, contains  $\leq$ 250 ppm monomethyl ether hydroquinone as inhibitor, 97%, MW = 130.14 g mol<sup>-1</sup>), IBOMA (80%, MW = 222.32 g mol<sup>-1</sup>), LA (90%, MW = 240.38 g mol<sup>-1</sup>), ammonia (NH<sub>3</sub>, anhydrous, 99.98%, MW = 17.03 g mol<sup>-1</sup>), sodium lauryl sulfate, SDS (98%, MW = 288.38 g mol<sup>-1</sup>), 2-acrylamido-2-methylpropane sulfonic acid (AMPS, 99%, MW = 207.25 g mol<sup>-1</sup>), polyvinyl alcohol (PVA, ash 0.5%, viscosity 10 mPa s, 4% in water, 20 °C, MW = 49.000 g mol<sup>-1</sup>), starch from wheat (unmodified), acetonitrile (ACN, MW = 41.05 g mol<sup>-1</sup>), tetrahydrofuran (THF, MW = 72.11 g mol<sup>-1</sup>), dimethyl sulfoxide-d (DMSO-d<sub>6</sub>, MW = 84.17 g mol<sup>-1</sup>), and chloroform-d (CDCl<sub>3</sub>, MW = 120.38 g mol<sup>-1</sup>) were purchased from Sigma-Aldrich and used as received unless specifically noted.

Grey concrete for masonry (contains Portland concrete) was instead purchased from Bricoman.



**Scheme 1.** Monomer combination for the production of core-shell NPs with a soft core and a harder shell. The relative monomer content refers to weight fractions. The process is conducted in one pot exploiting the cores as seeds to grow the shell. a) Monomer fractions and reaction procedure for LA-IBOMA samples; b) monomer fractions and reaction procedure for HEMALA<sub>4</sub>-ST samples.

## 2.2. Synthesis of HEMALA<sub>4</sub> via Ring Opening Polymerization

The degradable macromonomer HEMALA<sub>4</sub> was synthesized by ROP of lactide (Lac), using HEMA as initiator. The average number of lactoyl units was set to 4 by adjusting the Lac/HEMA mole ratio to 2. More specifically, 2.21 g of Lac (15.3 mmol) were melted in a round bottom flask at 130 °C. Then, 1.0 g of HEMA (7.7 mmol) and 16 mg of Sn(Oct)<sub>2</sub> (38 μmol, i.e., 1/200 mol mol<sup>-1</sup> with respect to HEMA) were mixed together and injected in the flask. The mixture was left at 130 °C for 2 h while stirring with a magnetic stirrer at 300 rpm. The reaction was finally quenched by cooling in a water/ice mixture. An aliquot of the product was then dissolved in deuterated chloroform at a concentration of 25 mg mL<sup>-1</sup> and analyzed via proton nuclear magnetic resonance (<sup>1</sup>H NMR) performed on a Bruker spectrometer operated at 400 MHz, with 32 scans per sample. The NMR spectrum of the product is shown in Figure S1 (Supporting Information) and, based on peak integration, the monomer conversion and average degree of polymerization were determined through Equations (S1)–(S4) (Supporting Information).

## 2.3. LA-IBOMA and HEMALA<sub>4</sub>-ST Core-Shell NP Synthesis

Semibatch free-radical emulsion polymerization conducted in one pot was exploited to synthesize the core-shell polymer NPs according to **Scheme 1**.

The reactions were carried out in a three-neck 500 mL round bottom flask stirred with a PTFE anchor connected to an impeller. The rotation speed was set to 200 rpm and the reaction was kept under nitrogen flux for the entire process duration. A condenser was added to control the solvent evaporation while one neck was used to feed the pre-emulsion.

In a typical formulation, reported as an example, as first step, the flask was charged with a solution of 3.33 g of AMPS (16 mmol), a charged monomer expected to provide colloidal stability to the NPs, and 83 g of deionized water. The pH was ad-

justed to 8 by addition of a 33% v/v ammonia solution and the flask was heated up to 55 °C.

In a separate flask, the pre-emulsion was prepared adding 45 g of LA (187 mmol), 15 g of IBOMA (67 mmol), 1.33 g of AMPS (6 mmol), 1.2 g of SDS (4 mmol), 83 g of deionized water, and 33 g of ethanol. As in the first flask, the pH was adjusted to 8. The pre-emulsion was then stirred until reaching a homogeneous suspension. Once reached homogeneity, 0.9 g of  $\alpha$ - $\alpha$  (3 mmol) dissolved in 3 mL of deionized water were added to the 500 mL flask, followed by the pre-emulsion, fed in 2 h with a peristaltic pump (NE-9000, NewEra Pump Systems) while keeping it stirred. After the addition was completed, the reaction was let to proceed in batch mode for further 2 h.

The polymer shell was added by feeding fresh monomer and initiator without interrupting the reaction. A second pre-emulsion with LA, IBOMA, AMPS, SDS, and deionized water was prepared and fed in 1 h. The amount of the different reactants depended on the desired shell thickness. For instance, to obtain a shell of 20 nm, 1.18 g of LA (5 mmol), 9.6 g of IBOMA (43 mmol), 0.72 g of AMPS (3 mmol), 0.21 g of SDS (0.7 mmol), and 11.5 g of deionized water were used. This time, the initiator (0.16 g of  $\alpha$ - $\alpha$  (0.6 mmol) in 1 mL of deionized water) was added drop by drop with the same feeding time as for the pre-emulsion. After the feeding was completed, the reaction was then left to proceed for one additional hour to reach total conversion.

The reaction was repeated with different monomer ratios to obtain a set of NPs with different shell thickness. The amount of monomer needed to obtain a desired shell thickness depends on the particle core size and was calculated as explained in the Supporting Information [see Equation (S5), Supporting Information].

A similar procedure was adopted to produce HEMALA<sub>4</sub>-ST NPs, with HEMALA<sub>4</sub> and ST replacing LA and IBOMA, respectively. To increase the bio-based content in this case, the core is obtained with HEMALA<sub>4</sub> only. For a similar reason, the shell was synthesized by feeding a monomer mixture comprising 75% w/w ST and 25% w/w HEMALA<sub>4</sub>, ensuring high bio-based content

and sufficiently high  $T_g$ . The surfactants, initiator, and process conditions are the same as reported for the LA-IBOMA samples.

## 2.4. Polymer Characterization

Aliquots of the reaction mixture were sampled every hour to measure the polymer nanoparticle size distribution, either as pure cores or as core-shell, via dynamic light scattering (DLS), performed on a Malvern Zetasizer Nano ZS instrument at a scattering angle of  $173^\circ$  (backscatter). The average size and polydispersity indexes (PDI) were reported as a function of time. The reported data are an average of three independent measurements.

The monomer conversion was assessed hourly by both thermogravimetric analysis and  $^1\text{H}$  NMR. The thermogravimetric analysis was conducted on an Ohaus MB120 moisture analyzer, set to  $100^\circ\text{C}$ .  $^1\text{H}$  NMR spectra were recorded on a Bruker 400 MHz spectrometer, with 32 scans per sample. The polymer suspension was first dried under a flow of air and then the polymer dissolved, at a concentration of  $20\text{ mg mL}^{-1}$  in deuterated chloroform for the analysis. A representative NMR spectrum of LA-IBOMA particles is reported in Figure S2 (Supporting Information).

The glass transition temperature ( $T_g$ ) of the produced copolymers was measured via differential scanning calorimetry (DSC), performed on a METTLER Toledo Polymer DSC using 10 mg of sample in 40  $\mu\text{L}$  aluminium crucibles, heating and cooling at the rates of  $10^\circ\text{C min}^{-1}$  in nitrogen atmosphere, with temperature ranging from room temperature to  $+125^\circ\text{C}$ . In order to remove residual stresses, the sample was first heated at  $10^\circ\text{C min}^{-1}$  to  $125^\circ\text{C}$  and then rapidly cooled down again to room temperature before the actual measurement.  $T_g$  was obtained from the DSC plot (heat flow vs temperature) using the inflection point in which the tangent to the curve changed its angular coefficient.

## 2.5. Spray Drying

The spray drying of the core-shell NPs was conducted on the Buchi Mini Spray Dryer B-290. The inlet temperature of the spray dryer was set to  $130^\circ\text{C}$ , resulting in an outlet temperature of  $80^\circ\text{C}$ . The peristaltic pump deputed to the feeding of the polymer suspension was set to a flow rate of  $10\text{ g min}^{-1}$ , the spray nozzle to 4 bar of  $\text{N}_2$ , and the aspiration at  $35\text{ m}^3\text{ h}^{-1}$ .

To avoid particle coalescence during the drying phase, PVA was added in powder form to the nanoparticle suspension in different amounts. The optimum was considered as the lowest amount of additive possible to obtain a redispersible powder.

Scanning electron microscopy (SEM) was conducted to monitor the particle morphology and size distribution. The images were taken at an electron high tension (EHT) of 20.00 kV on a Zeiss EVO 50 XVP microscope at a magnification of 2.5 k $\times$ .

## 2.6. Degradation Test

A solution that mimics the ion-rich water inside the pores of concrete was formulated to check the degradation of the RDPPs after spray-drying. NaOH ( $2610\text{ mg L}^{-1}$ ), KOH ( $9043\text{ mg L}^{-1}$ ), and

$\text{Ca}(\text{OH})_2$  ( $166.4\text{ mg L}^{-1}$ ) were dissolved in water to create an alkaline environment and 10 mg of each polymer powders were dispersed in 10 mL of solution and kept under stirring for two weeks.<sup>[26,27]</sup> The degradation was evaluated by tracking the particle size distribution at different time points. To measure it, DLS was performed on a Malvern Zetasizer Nano ZS instrument at a scattering angle of  $173^\circ$  (backscatter). The average size and PDI were reported as a function of time. The reported data are an average of three independent measurements.

## 2.7. Concrete Test

To evaluate the possibility of using the produced bio-based core-shell NPs as concrete additives, they were mixed with commercial concrete and the performances qualitatively monitored by evaluating the mixture morphology. Concrete and water were mixed at a 1:2 weight ratio. Then, the selected particles were added to the mixture in two different percentages: 5% and 15%  $w_{\text{polymer}}/w_{\text{concrete}}$ .

Water, cement, and polymer particles were mixed for 1 h with a stirrer and spread on a polystyrene surface. The mixtures were left to rest for 28 d. After this period, the concrete surface morphology was studied through optical microscopy (Leica Compound Microscope DM LM 020-520-718, magnification 5 k $\times$ ) and SEM.

## 3. Results and Discussion

First, to assess the possibility of synthesizing RDPPs with high bio-based content, lauryl acrylate was used as the main monomer to form the core of the core-shell system due to its hydrophobicity and low glass transition temperature, hence sticking ability. Lauryl acrylate in fact can be produced from vegetable oils thus contributing for the 80% to the chemicals from renewable sources. On the other hand, isobornyl methacrylate was selected to build a hard, thin shell around the core to protect it from particle interpenetration and fusion at the high temperatures reached during the drying phase. Both monomers have a high bio-based content, leading the core-shell NPs to be bio-renewable for more than 70% (see Table 1).

In particular, this bio-based carbon content was calculated as the amount of bio-derived carbon over the total number of carbons [Equation (1)].<sup>[28,29]</sup>

$$\text{Bio-based carbon content (\%)} = \frac{\text{Bio-derived organic carbon}}{\text{Total organic carbon}} * 100 \quad (1)$$

At the same time, to demonstrate that bio-based RDPPs could also be made degradable, HEMALA<sub>4</sub> was used to synthesize the core of the NPs, while styrene, leading to a harder polymer, as the main constituent of the shell. HEMALA<sub>4</sub> was synthesized by ROP using HEMA as initiator and Lac as the monomer. This in turn is typically obtained by lactic acid, a bio-based molecule produced through the fermentation of biomasses and showing high biocompatibility as it is a main player in the Krebs cycle of aerobic organisms. The molar ratio of lactide to HEMA can be

**Table 1.** List of synthesized samples and their characteristics. LA-IB are made of lauryl acrylate and isobornyl methacrylate while HL-ST are from HEMALA<sub>4</sub> and styrene. The target shell thickness is the input used in Equation (S5) (Supporting Information) to determine the amount of monomer required for the shell. The polydispersity index (PDI) and average size are obtained via DLS. The bio-based percentage is calculated considering the number of carbons from renewable sources over the total number of carbons in the molecule [Equation (1)].

Sample name	Core size [nm]	Final size [nm]	Target shell thickness [nm]	Shell thickness [nm]	PDI <sub>core</sub> [-]	PDI <sub>core-shell</sub> [-]	Bio-based content [%]
LA-IB1	220 ± 11	238 ± 15	10	9	0.010 ± 0.003	0.010 ± 0.005	76
LA-IB2	191 ± 20	255 ± 16	25	32	0.090 ± 0.005	0.060 ± 0.009	75
HL-ST1	127 ± 16	145 ± 12	10	9	0.050 ± 0.010	0.060 ± 0.011	57
HL-ST2	105 ± 8	155 ± 17	25	25	0.020 ± 0.004	0.050 ± 0.010	33

conveniently modified to tune the length of the macromonomer, which has a major impact on its thermomechanical properties and degradation time. In fact, the degradation occurs by hydrolysis of the ester bonds in the macromonomer, as demonstrated in other works.<sup>[30–32]</sup> Therefore, this parameter can be adjusted based on the desired application. In this work, HEMALA<sub>4</sub> was selected based on previous experience in order to ensure good filming properties, degradation time compatible with the application as cement additive and good handling, important when going to industrial settings.<sup>[24,32]</sup> The conversion and average chain length of this degradable macromonomer were determined via <sup>1</sup>H NMR, as shown in Figure S1 (Supporting Information). Conversions of 97% and 96% were reached for HEMA and lactide, respectively. Finally, the mean number of lactoyl repeating units, set to 4, was found to be 3.6.

For both the systems, LA-IB and HL-ST, samples with different shell thickness were synthesized to find the best optimum between shell protection during drying and filming ability, taking into account a previous study that assessed 10 nm as the minimum thickness needed to properly shield the core.<sup>[13]</sup> To calculate the amount of monomer to be added for the synthesis of the shell, we relied on Equation (S5) (Supporting Information), which imposes the preservation of the number of nanoparticles. The samples produced with their main features are listed in Table 1, where the measured shell thickness has been evaluated by halving the difference between the diameters of the core-shell NPs and of the cores, both measured via DLS.

The monomer conversion and NP size for the four reported formulations were tracked during the polymerization and are reported in Figure 1. In all cases, the semibatch approach allowed to access starved monomer conditions, as inferred by the local cumulative conversion reaching a plateau at very high values (i.e., >99%) during the feeding phase. This also ensured a complete monomer conversion during the following batch phase. A plateau was reached after 2 h also by the average particle size. After 4 h, the addition of the shell-forming monomers started, exploiting the cores as nuclei in a one-pot process. As expected, a step increase in the NP size was observed after the addition of the shell. For all the samples, the DLS analysis revealed a unimodal and narrow particle size distribution (Figure S3a, Supporting Information), suggesting the avoidance of a secondary nucleation after the addition of the shell. This consideration is further supported by the number of nanoparticles in the reaction medium that remained constant throughout the two-step process, as shown in Figure S3b (Supporting Information) for the sample LA-IB1, as an example. It is then possible to conclude

that the core-shell structure could be properly obtained with this process. Interestingly, smaller NPs were obtained for HL-ST samples with respect to the LA-IB ones.

The possibility of obtaining suitable RDPPs is governed by the  $T_g$  of the shell. In fact, this should be higher than the drying temperature in order to prevent irreversible coalescence of the NPs. For this reason, monomers leading to high  $T_g$  polymers, namely, IBOMA and styrene, were selected to produce the shell. At the same time, to favor the interactions between the core and the shell and avoid renucleation, 25% w/w of the “hard” monomer IBOMA was also included in the core, in the case of the LA-IB samples (Table 2). Regarding HL-ST NPs instead, the goal was to make them as degradable and bio-based as possible. For this reason, no styrene was added to the core of the HL-ST samples, which were realized completely with HEMALA<sub>4</sub>. On the other hand, to make the shell compatible with the core, the highest mass fraction possible of the “soft” monomer was included in the shell formulation. This maximum mass fraction of LA or HEMALA<sub>4</sub> that could be added to the shell was estimated based on the Fox equation [Equation (2)], considering that the outlet temperature of the spray drying adopted to produce the powder from the NP latexes was 80 °C. This temperature was then considered as the minimum allowable  $T_g$  for the shell-forming copolymer.

$$\frac{1}{T_g} = \frac{\omega_{m_1}}{T_{g_1}} + \frac{\omega_{m_2}}{T_{g_2}} + \dots + \frac{\omega_{m_n}}{T_{g_n}} \quad (2)$$

where  $T_g$  is the glass transition temperature of the final copolymer,  $T_{g_i}$  is the one of homopolymer *i*, and  $\omega_{m_i}$  is the weight fraction of monomer *i* in the final copolymer. From this analysis, the maximum amount of LA that could be incorporated in the shell of LA-IB samples to reach a  $T_g$  of 80 °C was 11% w/w, while for HEMALA<sub>4</sub> this maximum content was 25% w/w, which contributed to increase the overall bio-based content of the HL-ST samples (Table 2).

The  $T_g$  of the core and core-shell systems was measured via DSC. In particular, the  $T_g$  was taken as the inflection point of the heat flow versus temperature thermogram measured for the samples. These curves are reported in Figure 2 for the core-shell NPs produced with the thickest shell, namely, LA-IB2 and HL-ST2, as an example.

From the figure, it is possible to observe that a  $T_g$  close to the value expected from the Fox equation (i.e., 80 °C, see Table 2) was measured, which is much higher than the one for the core and confirms that the shell properly shields the thermal behav-

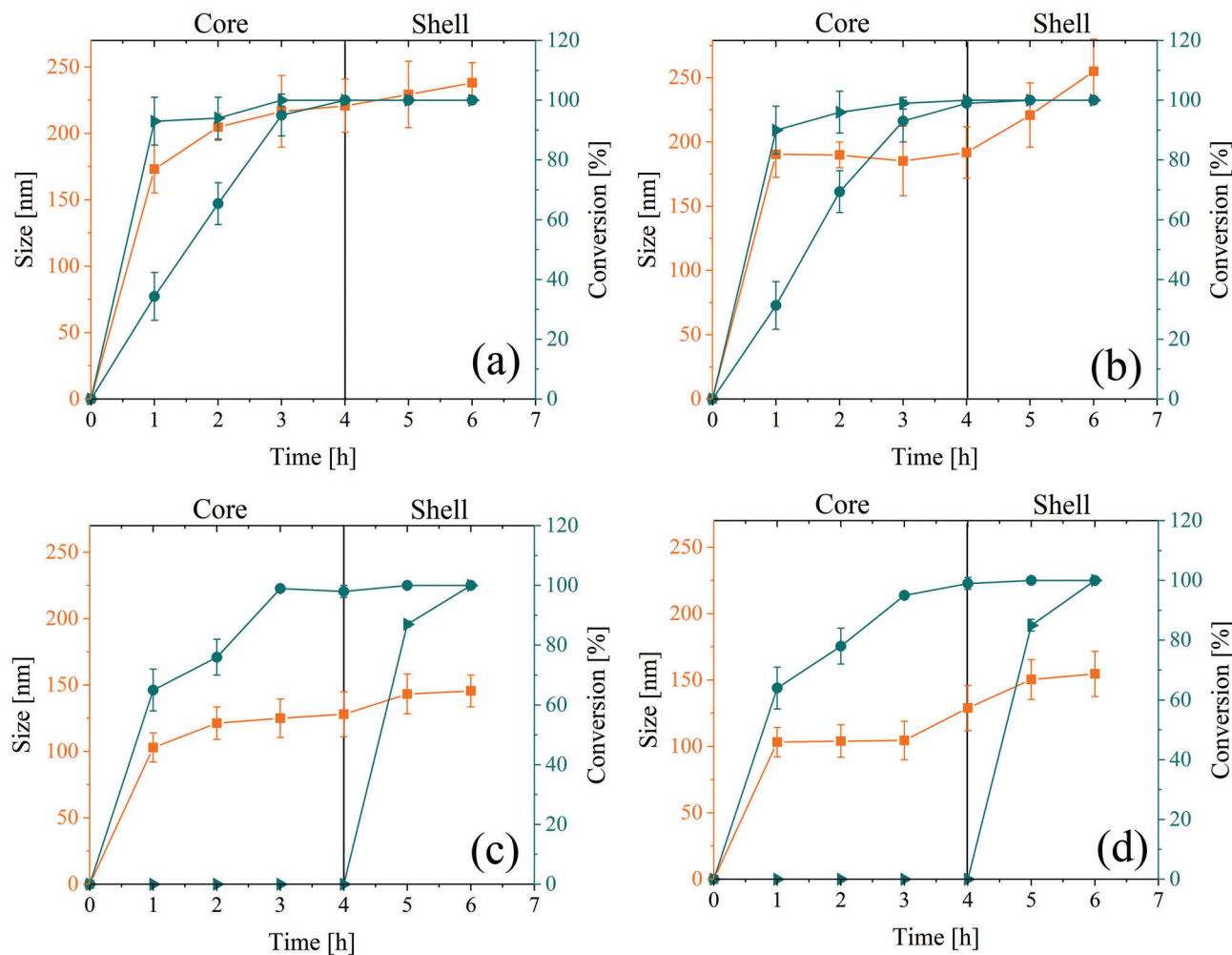


**Figure 1.** Particle size (■) and “soft” (●) and “hard” (►) monomer conversion for a) LA-IB1, b) LA-IB2, c) HL-ST1, and d) HL-ST2.

**Table 2.** Core and shell monomer distribution and glass transition temperatures for the four samples produced.

Sample	Core mon. ratio	Shell mon. ratio	$T_{g_{core}}$ [°C]	Target $T_{g_{shell}}$ [°C]	$T_{g_{shell}}$ [°C]
LA-IB1	75:25	11:89	-28	80	77
LA-IB2	75:25	11:89	-28	80	78
HL-ST1	100:0	25:75	33	80	84
HL-ST2	100:0	25:75	33	80	77

ior of the softer core.<sup>[33–35]</sup> This is important when aiming at the production of RDPPs, as it ensures the proper protection from the heating and consequent coalescence that the core would be subjected to during the drying process. It is worth noticing that for the sample HL-ST2, two steps can be observed in the thermogram, associated to two values of  $T_g$ , i.e., 77 and 98 °C. This might be due to a certain compositional drift in the shell, driven by different reactivities of HEMALA<sub>4</sub> and styrene. However, both are much higher than the  $T_g$  measured for the core, i.e., 33 °C, which supports its proper shielding.

After the characterization of the core–shell NPs, the polymer latexes were spray dried in a Buchi Mini Spray Dryer B-290. For a successful drying without coalescence, in addition to a high- $T_g$  shell, a redispersion co-adjuvant is usually required to increase the particle redispersibility and decrease agglomeration.<sup>[36]</sup> PVA is mainly used for this purpose, in concentrations ranging from 5 to 10% w/w over the polymer. Redispersibility tests were then performed in the absence or presence of PVA to evaluate its impact during the spray drying. The amount of stabilizer added as a powder to the NP suspension before drying is listed in Table 3, together with the particle size before and after drying and redispersion. In particular, the predrying particle size refers to the average NP size after the addition of the stabilizer.

In order to conclude about the redispersibility of the core–shell NPs after drying, we relied on the average size and polydispersity index measured via DLS (see Table 3).

Independently on the polymer used, when no stabilizer was added to the formulation, an irreversible coagulation was observed, with the consequent impossibility of redispersing the particles in water. The presence of PVA in most of the cases was able to prevent an irreversible polymer coagulation. The difference between a well-dispersed, fine powder and particle agglomera-

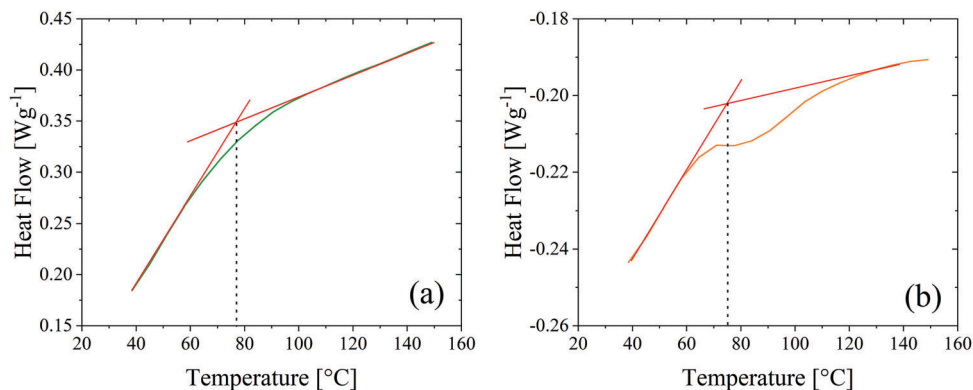


**Figure 2.** Thermograms measured via DSC, with a heating rate of  $10\text{ }^{\circ}\text{C min}^{-1}$  for a) LA-IB2 and b) HL-ST2.

**Table 3.** List of samples with different percentage of PVA as stabilizer and their size and polydispersity index in water after redispersion.

Sample	PVA/Polymer [%]	Pre-drying size [nm]	Post-drying size [nm]	Post-drying PDI [-]
LA-IB1	0%	$238 \pm 15$	Large aggregates	
LA-IB1	10%	$244 \pm 17$	$488 \pm 32$	$0.109 \pm 0.054$
LA-IB1	5%	$244 \pm 19$	$471 \pm 67$	$0.382 \pm 0.092$
LA-IB2	0%	$255 \pm 16$	Large aggregates	
LA-IB2	10%	$295 \pm 23$	$968 \pm 101$	$0.255 \pm 0.032$
LA-IB2	5%	$294 \pm 15$	$957 \pm 121$	$0.401 \pm 0.103$
HL-ST1	0%	$145 \pm 12$	Large aggregates	
HL-ST1	10%	$147 \pm 18$	$2023 \pm 201$	$0.11 \pm 0.091$
HL-ST1	5%	$145 \pm 17$	Large aggregates	
HL-ST2	0%	$155 \pm 17$	Large aggregates	
HL-ST2	10%	$159 \pm 21$	$1827 \pm 232$	$0.725 \pm 0.204$
HL-ST2	5%	$156 \pm 18$	$1100 \pm 154$	$0.440 \pm 0.113$

tion was visible even to the naked eye as shown in **Figure 3**. This difference was confirmed by the ability of the particles to redisperse in water (Figure S4, Supporting Information): while in the first case the powder redispersed greatly, in the second the pres-

ence of floating aggregates is clearly visible. As already stated, the postdrying size and PDI of the redispersible samples have been reported in Table 3: an increase in both the parameter has been registered for all the particles but LA-IB samples seem to better resist the drying process because their size and dispersion did not vary as much as the HL-ST ones.

This distinction in the drying response could derive from both the difference in the material or in the particle size, because HL-ST particles have smaller size and hence greater surface area available, which favors the coalescence.

The NP agglomeration was also tracked by analyzing their morphology via SEM. Particles with no PVA are shown in **Figure 4a**. Here, the formation of flake-like aggregates is clearly visible, with the primary NPs losing their identity. On the other hand, two different conformations were observed for the redispersible particles: while LA-IB1, LA-IB2, and HL-ST1 have the spherical, well-defined morphology shown in Figure 4b as an example, most of HL-ST2 particles showed an exploded morphology (Figure 4c).

This is surprising considering that HL-ST2 has a relatively thick shell that should ensure resistance to the high temperatures reached during the drying phase. On the other hand, HL-ST1 with only 10 nm as shell led to spherical particles after resuspension. A hypothesis for this behavior is that the thick, hydrophobic

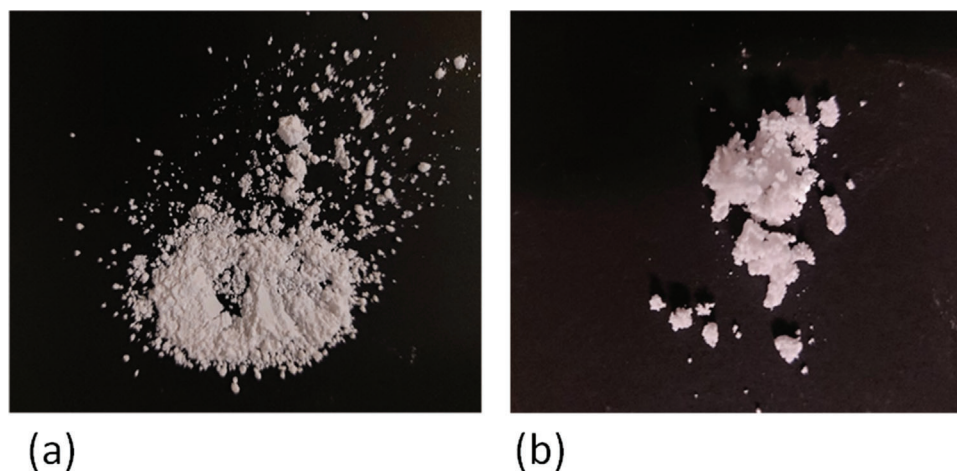
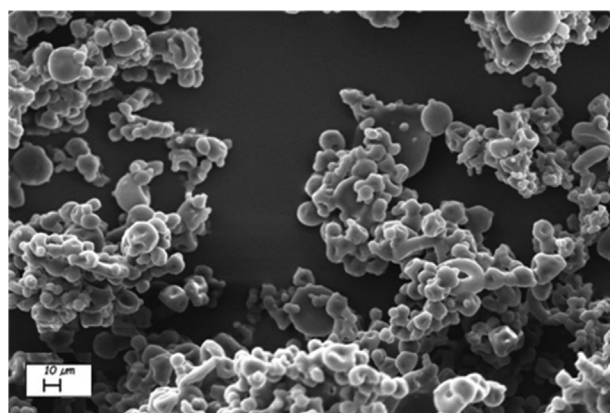
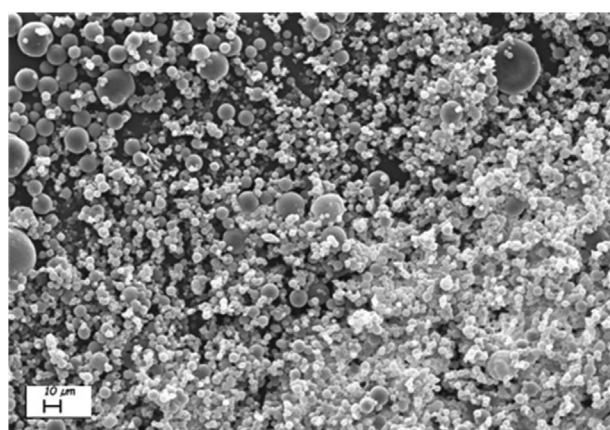


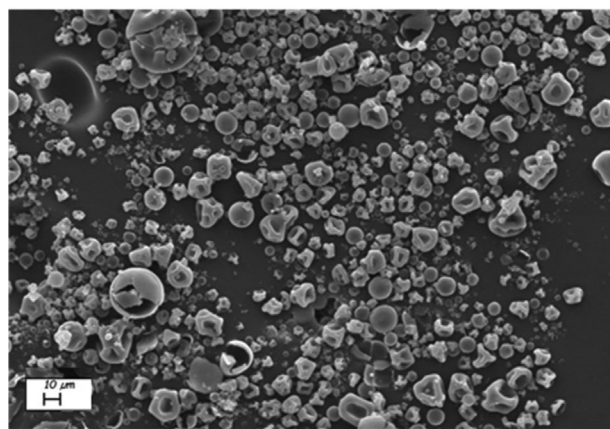
**Figure 3.** Particles after spray drying process: a) dried powder and b) particle agglomeration.



(a)



(b)



(c)

**Figure 4.** SEM images of a) HL-ST1 with no PVA – agglomerated particles, b) HL-ST1 with 10% PVA – spherical and well-dispersed particles, and c) HL-ST2 NPs with 10% PVA showing an exploded morphology. The images were recorded at an EHT of 20.00 kV and magnification = 2.500 kx.

outer layer made of styrene could have prevented the particle core to dry properly, as better explained by the Biot theory.

Indeed, Biot number  $Bi^{[37]}$  in Equation (3), describes the relationship between the tendency of the particle to exchange heat

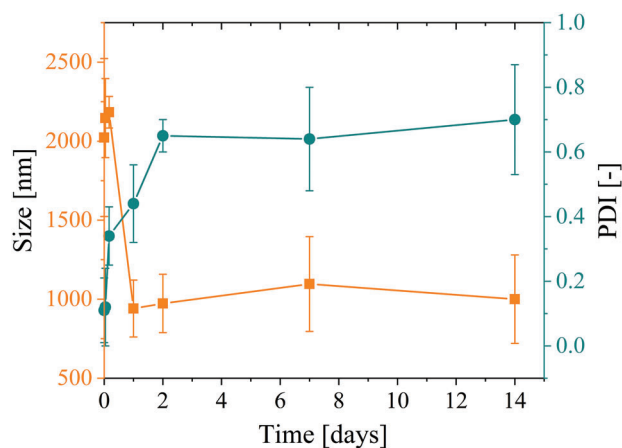


**Figure 5.** HL-ST1 particle size (■) and PDI (●) variation over time in alkaline solution (pH = 10).

with the outside (in this case the nitrogen flux) with respect to the propensity to conduce heat inside

$$Bi = \frac{\text{external convection}}{\text{internal conduction}} = \frac{hD_p}{\lambda} \quad (3)$$

where  $h$  is the heat transport coefficient,  $\lambda$  is the thermal conductivity of the particle material, and  $D_p$  its diameter. If  $Bi$  is greater than 1, the particles dry easily on the surface but the heat is conducted very slowly inside the particle. This causes the formation of a hydrophobic dry outer layer that entraps the water inside, preventing uniform drying. The evaporation of this water combined with the hardness of the shell causes the particle to break or deform. For this reason, a too thick outer shell made of a hydrophobic, hard material could have led to the particle explosion.

An additional feature of the HEMALA<sub>4</sub>-based RDDPs is the degradability in aqueous environments, occurring through hydrolysis of the ester bonds in the macromonomer. To verify this behavior, the particle size distribution of HL-ST1 has been tracked after redispersion in an alkaline environment simulating the water in the pores of concrete. The degradation has been followed for two weeks and the results are reported in **Figure 5**.

Both PDI and size undergo an abrupt change during the first 2 d, while remaining almost constant afterward. In particular, the average particle size almost halves, going from 2023 to 1005 nm. This can be considered a proof of the degradation of the polyester material, which in turn leads to a particle shrinkage. In addition, the polydispersity increase suggests that the degradation is also accompanied by a certain extent of aggregation of the polymer material, which perturbs the homogeneity of the original sample. It can be concluded that, since the particles reduce their size by 50%, they should be able to create voids inside concrete, an interesting feature for aerants. As a control, a similar analysis was also performed on the LA-IB1 sample that does not contain cleavable ester bonds (Figure S5, Supporting Information). Except for an initial NP swelling, in this case the particle size decreases to a much lower extent (<10%) compared to the HL-ST1 sample, confirming the expected poor degradability of this material.

Given the discussion so far, LA-IB1 and HL-ST1 were selected for preliminary tests with concrete since they possess both good



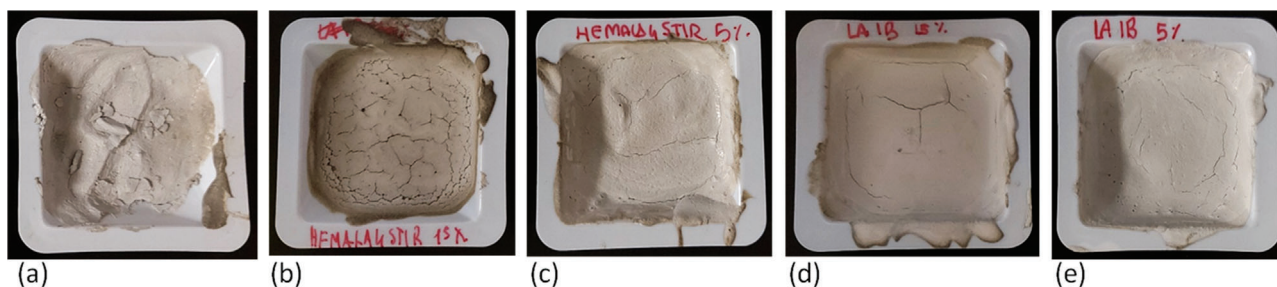


**Figure 6.** a) Reference, b) concrete with 15% of HL-ST1, c) concrete with 5% of HL-ST1, d) concrete with 15% of LA-IB1, and e) concrete with 5% of LA-IB1.

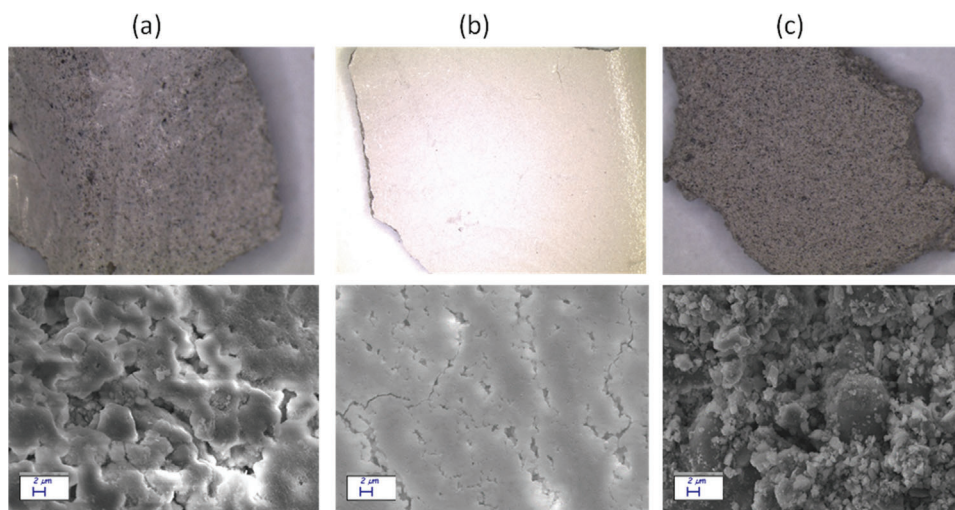


**Figure 7.** a) Reference, b) concrete with 15% of LA-IB1, and c) concrete with 15% of HL-ST1. Top row: optical microscope images (25 $\times$ ); bottom row: SEM images recorded at an EHT of 20.00 kV and magnification of 5.00 kx.

redispersibility and morphology. In addition, thinner shell implies higher bio-based content especially for the HL-ST system, as reported in Table 2.

Concerning these tests, two concrete samples for each additive were prepared by mixing grey concrete cement with 5% and 15% w/w of dried particles. After maturation for 28 d, these samples were compared to a reference without additives (**Figure 6a**).

Generally, a better miscibility and more homogenous surface were found for all the samples compared to the reference one. This confirms the suitability of the developed RDPPs to act as concrete additives. However, the behavior introduced by the two samples was opposite. While for LA-IB a smoother and compacter surface was found, the sample with HL-ST is much more cracked. This is certainly due to the different nature of the additives. This difference in the surface aspect of the reference and the samples with 15% w/w of RDPPs was further investigated through optical microscope and SEM, as shown in **Figure 7**.

SEM and optical microscope images confirmed the creation of a smoother and more compact surface compared to the reference when LA-IB NPs were added to the concrete. As visible from the microscopy image, the additive caused a more coalesced surface structure, favoring the fusion of the grains in the concrete. As a matter of fact, while in the reference sample individual grains can still be detected, these are almost completely fused together

when LA-IB1 was added. This suggests that these NPs might be potential candidates as waterproof agents, reducing the overall porosity of the system. On the other hand, the addition of HL-ST NPs led to the formation of hole-enriched concrete as clearly visible from **Figure 7c**. Here, the additive appeared to prevent the concrete grain fusion. In fact, small individual particles can still be observed from the microscopy image of the sample treated with HL-ST1. This led to an improved porosity and void fraction compared to the reference sample. Therefore, these NPs could be potential candidates as air-entrainment additives. Nevertheless, holes creation increases the friability of the material and further studies should focus on finding the optimum between the two parameters.

These preliminary experiments suggest that the bio-based materials reported herein could be adopted as RDPPs in the cement sector. However, more detailed characterizations, starting from the evaluation of the mechanical properties of the cement-additive mixture, have to be put in place in order to claim about their efficacy as cement additives.

## 4. Conclusions

In this work, we report the synthesis of RDPPs with high bio-based content that might be adopted for two different purposes:

as waterproofing agents or air-entrainment additives. The former, nondegradable, is made of lauryl acrylate and isobornyl methacrylate while the second, due to the presence of poly(lactic acid), can degrade in aqueous environments especially at alkaline pH, like in the case of concrete. The two set of additives have been synthesized via a two-step emulsion polymerization in water to create core-shell particles with softer core and harder shell. The procedure has been optimized and particles with different shell thickness have been produced to find the best performance in terms of sprayability. Indeed, the particles were dried with a spray dryer to create an easy-to-handle powder that could be mixed directly with concrete and the desired amount of water. A preliminary trial to verify the particle miscibility with concrete and the obtained material characteristics has been carried out creating mixtures with different percentages of additives over concrete. The surface sample morphology was then studied at SEM finding a more compact and smoother surface in the former case and highly porous concrete in the latter. Further studies should focus on the optimization of the additive amount and on water-permeability and mechanical performances.

## Supporting Information

Supporting Information is available from the Wiley Online Library or from the author.

## Conflict of Interest

The authors declare no conflict of interest.

## Data Availability Statement

The data that support the findings of this study are available from the corresponding author upon reasonable request.

## Keywords

bio-based polymers, core-shell nanoparticles, emulsion polymerization, redispersible polymer powders, spray-drier

Received: July 1, 2022

Revised: August 14, 2022

Published online: October 3, 2022

- [1] M. Moreno, J. I. Miranda, M. Goikoetxea, M. J. Barandiaran, *Prog. Org. Coat.* **2014**, *77*, 1709.
- [2] J. Chauvet, J. M. Asua, J. R. Leiza, *Polymer* **2005**, *46*, 9555.
- [3] N. Manfredini, J. Ilare, M. Invernizzi, E. Polvara, D. Contreras Mejia, S. Sironi, D. Moscatelli, M. Sponchioni, *Ind. Eng. Chem. Res.* **2020**, *59*, 12766.
- [4] N. Manfredini, M. Merigo, J. Ilare, M. Sponchioni, D. Moscatelli, *Nanoscale* **2021**, *13*, 8543.

- [5] J.-Z. Ma, Y.-H. Liu, Y. Bao, J.-L. Liu, J. Zhang, *Adv. Colloid Interface Sci.* **2013**, *197*, 118.
- [6] Y.-Y. Yu, W.-C. Chien, T.-W. Tsai, H.-H. Yu, H. H. Yu, *Mater. Chem. Phys.* **2011**, *126*, 962.
- [7] M. P. L. Werts, M. Badila, C. Brochon, A. Hébraud, G. Hadziioannou, G. Hadziioannou, *Chem. Mater.* **2008**, *20*, 1292.
- [8] Y. Zheng, Y. He, Y. Qing, C. Hu, Q. Mo, *Appl. Surf. Sci.* **2013**, *265*, 532.
- [9] A. K. Khan, B. C. Ray, S. K. Dolui, *Prog. Org. Coat.* **2008**, *62*, 65.
- [10] F. Jasinski, V. L. Teo, R. P. Kuchel, M. M. Mballa, S. C. Thickett, R. H. G. Brinkhuis, W. Weaver, P. B. Zetterlund, *J. Polym. Sci., Part A: Polym. Chem.* **2017**, *55*, 2513.
- [11] R. G. Chaudhuri, S. Paria, *Chem. Rev.* **2012**, *112*, 2373.
- [12] N. Tarannum, K. Pooja, *Recent Trends and Applications in the Research and Development Activities of Redispersible Powder: A Vision of Twenty-First Century*, Springer, Berlin **2021**.
- [13] S. Caimi, E. Timmerer, M. Banfi, G. Storti, M. Morbidelli, *Polymers* **2018**, *10*, 1122.
- [14] N. Tarannum, K. Pooja, R. Khan, *Constr. Build. Mater.* **2020**, *247*, 118579.
- [15] A. J. Ango, K. Wan-Ki, S. Yang-Seob, *Proceedings of the Korea Concrete Institute Conference* **2003**, *11*, 252.
- [16] Statista. Cement Production Global 2020 | Statista, **2021**.
- [17] Rodgers L. Climate Change: The Massive CO<sub>2</sub> Emitter You May Not Know about - BBC News, *BBC News* **2018**.
- [18] C. Bories, E. Vedrenne, A. Paulhe-Massol, G. Vilarem, C. Sablayrolles, *Constr. Build. Mater.* **2016**, *125*, 1142.
- [19] C. G. Hoyos, R. Zuluaga, P. Gañán, T. M. Pique, A. Vazquez, *J. Clean. Prod.* **2019**, *235*, 1540.
- [20] Y. Zhang, Z. Jiang, Y. Zhu, J. Zhang, Q. Ren, T. Huang, *Constr. Build. Mater.* **2021**, *267*, 120551.
- [21] C. Ma, B. Chen, *Constr. Build. Mater.* **2016**, *113*, 255.
- [22] H. Sajjad, W. B. Tolman, T. M. Reineke, *ACS Appl. Polym. Mater.* **2020**, *2*, 2719.
- [23] C. Fang, X. Zhu, Y. Cao, X. Xu, S. Wang, X. Dong, X. Dong, *Int. J. Adhes. Adhes.* **2019**, *100*, 102623.
- [24] Y. Yu, R. Ferrari, M. Lattuada, G. Storti, M. Morbidelli, D. Moscatelli, D. Moscatelli, *J. Polym. Sci., Part A: Polym. Chem.* **2012**, *50*, 5191.
- [25] A. Vazquez, T. M. Pique, *Biotech Admixtures for Enhancing Portland Cement Hydration*, Elsevier, Amsterdam **2016**.
- [26] M. Khadra, N. Burlion, T. Rougelot, J.-P. Carlier, J.-F. Lataste, *Eur. J. Environ. Civ. Eng.* **2019**, *23*, 1413.
- [27] C. Li, Z. Jiang, R. J. Myers, Q. Chen, M. Wu, J. Li, P. J. M. Monteiro, *Cem. Concr. Compos.* **2020**, *111*, 103630.
- [28] E. Prandato, S. Livi, M. Melas, J. Auclair, V. Verney, E. Fleury, F. Méchin, *J. Polym. Sci., Part B: Polym. Phys.* **2015**, *53*, 379.
- [29] C. Zhang, H. Wang, W. Zeng, Q. Zhou, *Ind. Eng. Chem. Res.* **2019**, *58*, 5195.
- [30] M. Sponchioni, U. C. Palmiero, D. Moscatelli, D. Moscatelli, *Macromol. Chem. Phys.* **2017**, *218*, 1700380.
- [31] A. Cingolani, T. Casalini, S. Caimi, A. Klaue, M. Sponchioni, F. Rossi, G. Perale, *Polymers* **2018**, *10*, 851.
- [32] M. Maraldi, A. Guida, M. Sponchioni, D. Moscatelli, *Macromol. Mater. Eng.* **2021**, *306*, 2000592.
- [33] E. Kang, B. Graczykowski, U. Jonas, D. Christie, L. A. G. Gray, D. Cangialosi, R. D. Priestley, G. Fytas, *Macromolecules* **2019**, *52*, 5399.
- [34] T. Chang, H. Zhang, X. Shen, Z. Hu, Z. Hu, *ACS Macro Lett.* **2019**, *8*, 435.
- [35] R. R. Baglay, C. B. Roth, *J. Chem. Phys.* **2017**, *146*, 203307.
- [36] X. Chen, B. Zheng, J. Shen, J. Shen, *Drying Technol.* **2013**, *31*, 433.
- [37] X. D. Chen, X. Peng, X. Peng, *Drying Technol.* **2005**, *23*, 83.